Protein Structure and Folding:

Molecular Architecture and Functional Analysis of NetB, a Pore-forming Toxin from *Clostridium perfringens*

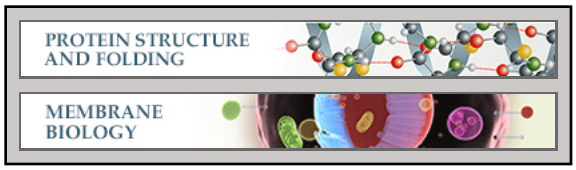

Christos G. Savva, Sérgio P. Fernandes da Costa, Monika Bokori-Brown, Claire E. Naylor, Ambrose R. Cole, David S. Moss, Richard W. Titball and Ajit K. Basak

J. Biol. Chem. 2013, 288:3512-3522.
doi: 10.1074/jbc.M112.430223 originally published online December 13, 2012

⌘ *Author's Choice*

THE JOURNAL OF BIOLOGICAL CHEMISTRY VOL. 288, NO. 5, pp. 3512–3522, February 1, 2013

Molecular Architecture and Functional Analysis of NetB, a Pore-forming Toxin from *Clostridium perfringens*[*] [S]

Received for publication, October 23, 2012, and in revised form, December 12, 2012 Published, JBC Papers in Press, December 13, 2012, DOI 10.1074/jbc.M112.430223

Christos G. Savva[‡1], Sérgio P. Fernandes da Costa[§1], Monika Bokori-Brown[§], Claire E. Naylor[‡], Ambrose R. Cole[‡], David S. Moss[‡], Richard W. Titball[§2], and Ajit K. Basak[‡3]

From the [‡]Department of Biological Sciences, School of Crystallography, Institute of Structural and Molecular Biology, Birkbeck College, Malet Street, London, WC1E 7HX, United Kingdom and the [§]College of Life and Environmental Sciences, University of Exeter, Stocker Road, Exeter, EX4 4QD, United Kingdom

Background: *Clostridium perfringens* toxin NetB is a key factor in avian necrotic enteritis.
Results: NetB forms heptameric pores structurally similar to *Staphylococcus aureus* toxins but lacks a phosphocholine binding pocket. NetB activity is enhanced by cholesterol.
Conclusion: NetB has distinct binding specificity, and cholesterol may act as a receptor.
Significance: The structure of NetB will facilitate development of control measures against necrotic enteritis.

NetB is a pore-forming toxin produced by *Clostridium perfringens* and has been reported to play a major role in the pathogenesis of avian necrotic enteritis, a disease that has emerged due to the removal of antibiotics in animal feedstuffs. Here we present the crystal structure of the pore form of NetB solved to 3.9 Å. The heptameric assembly shares structural homology to the staphylococcal α-hemolysin. However, the rim domain, a region that is thought to interact with the target cell membrane, shows sequence and structural divergence leading to the alteration of a phosphocholine binding pocket found in the staphylococcal toxins. Consistent with the structure we show that NetB does not bind phosphocholine efficiently but instead interacts directly with cholesterol leading to enhanced oligomerization and pore formation. Finally we have identified conserved and non-conserved amino acid positions within the rim loops that significantly affect binding and toxicity of NetB. These findings present new insights into the mode of action of these pore-forming toxins, enabling the design of more effective control measures against necrotic enteritis and providing potential new tools to the field of bionanotechnology.

For decades antibiotics have been added to animal feedstuffs, leading to enhanced weight gain and more efficient conversion of feed into body mass (1). However, there are concerns that the addition of antibiotics to animal feedstuffs contributes to the spread of antibiotic resistance. Consequently, the use of antibiotics as growth promoters has been banned in some countries (2). The reduction in the use of antibiotic growth promoters has had some unexpected consequences. Worryingly, some infectious diseases have become more widespread in livestock and are now emerging diseases. One of these diseases is necrotic enteritis in poultry, caused by the bacterium *Clostridium perfringens*. Acute necrotic enteritis is characterized by a sudden increase in flock mortality, and at necropsy necrotic foci are found in the intestinal mucosa. Chronic disease, which does not result in death, is less easily diagnosed (3–5). This form of the disease results in reduced weight gain in poultry (6, 7) and is likely to cause the greatest economic losses (8). The full impact of the reduction in antibiotic growth promoters on the incidence of necrotic enteritis is not yet known. However, it has been estimated that the current cost of necrotic enteritis to the international poultry industry is approximately 2 billion United States dollars a year (9, 10).

Recently, a newly discovered toxin from *C. perfringens*, termed NetB (necrotic enteritis toxin B-like), has been shown to play a major role in disease (11). The mode of action of this toxin is not fully understood, but Keyburn *et al.* (11) have shown that based on osmotic protection assays, NetB appears to form pores of ~1.7-nm diameter in Leghorn chicken hepatocellular carcinoma cells (LMH).[4] Importantly, a *netB* mutant of *C. perfringens* was unable to cause gut lesions in experimentally infected poultry (11). On the basis of limited sequence homology with other bacterial toxins, NetB is likely to be a member of the of β-pore-forming toxin (β-PFT) family. Respectively, NetB shares 30 and 25% sequence identity to *Staphylococcus aureus* α-hemolysin (αHL) and γ-hemolysin (γHL) component B (HlgB or LukF) and 38 and 40% sequence identity to the β and δ toxins of *C. perfringens* (supplemental Fig. 1). The heptameric structure of one of the most widely studied β-PFTs, *S. aureus* αHL, was determined more than 15

* This work was supported in part by Wellcome Trust Award WT089618MA (to D. M., Prof. H. Saibil, A. B., and R. T.). In addition, this work was supported by European Union Marie Curie Network Grant 237942 (to R. T.).
⌘ *Author's Choice*—Final version full access.
[S] This article contains supplemental Figs. 1–4.
The atomic coordinates and structure factors (code 4H56) have been deposited in the Protein Data Bank (http://wwpdb.org/).
[1] Both authors contributed equally to this work,
[2] To whom correspondence may be addressed: Biosciences, College of Life and Environmental Sciences, Geoffrey Pope Bldg., University of Exeter, Stocker Rd., Exeter, EX4 4QD, UK. E-mail: r.w.titball@exeter.ac.uk.
[3] To whom correspondence should be addressed. E-mail: a.basak@mail.cryst.bbk.ac.uk.

[4] The abbreviations used are: LMH, hepatocellular carcinoma cell; β-PFT, β-pore-forming toxin; αHL, α-hemolysin; γHL, γ-hemolysin; VCC, *V. cholerae* cytolysin toxin; hRBC and cRBC, human and chicken RBC; PG, phosphatidylglycerol; DOPC, dioleoylphosphatidylcholine; MPD, 2-methyl-2,4-pentanediol; Bis-Tris, 2-[bis(2-hydroxyethyl)amino]-2-(hydroxymethyl)-propane-1,3-diol.

years ago (12) and was until recently the only high resolution structure of a β-PFT in the membrane-inserted form. The ring-shaped complex resembles a mushroom, with the cap forming the extracellular domain and the stem forming the membrane-spanning region, in which each subunit contributes one β-hairpin. More recently, the structures of the bi-component, hetero-octameric complex of γHL from *S. aureus* (13), composed of four copies of LukF and Hlg2 (HlgA), and the cholesterol-requiring *Vibrio cholerae* cytolysin toxin (VCC) (14) were also determined by x-ray crystallography. Both toxins feature architectures common to αHL and demonstrate how distantly related toxins from different organisms adopt a similar pore-forming architecture.

Although NetB appears to form pores in target cell membranes, little is known about the molecular basis of toxicity, which hinders our ability to devise effective control measures against necrotic enteritis. In this study we report the crystal structure of the heptameric complex of NetB in detergent, which likely represents the membrane-inserted pore form. The active toxin adopts a similar conformation to αHL but displays important differences in the membrane binding region and the pore lumen that may influence its specificity and channel forming properties. In addition, we identified residues critical for NetB binding and toxicity and have shown that cholesterol is important for NetB activity. This work will provide the basis for the development of vaccines against necrotic enteritis and furthers our understanding of the mechanisms employed by this family of PFTs.

EXPERIMENTAL PROCEDURES

Molecular Cloning of the netB Gene—Bacterial genomic DNA from *C. perfringens* strain 56 (15) was isolated with the Wizard Genomic Purification kit (Promega) and used as a template to amplify the *netB* gene (UniProt accession number A8ULG6), which was subsequently cloned into the pBAD expression vector to generate recombinant pBAD-NetB. Thereby, NetB is expressed as a 331-amino acid protein without its native signal peptide, an N-terminal His tag to facilitate affinity purification, and an Xpress™-tag epitope for detection. In addition, the following NetB mutants were designed by site-directed mutagenesis: K77A, Y78A, Y79A, Y187A, H188A, Y191A, R200A, Y202A, W257A, E258A, and W262A. Mutants were made with the QuikChange II site-directed mutagenesis Kit (Stratagene) and verified by sequencing.

Expression and Purification of NetB in E. coli—*E. coli* carrying the pBAD-NetB vector was grown to an optical density ($A_{595\ nm}$) of 0.5, and expression of NetB was induced for 6 h by adding arabinose at a final concentration of 0.02% (w/v). Bacterial cells were harvested by centrifugation, and cells were lysed enzymatically by using BugBuster reagent (Novagen). NetB protein was purified by His-bind chromatography columns (GE Healthcare) according to the manufacturer's instructions. Subsequently, the protein was dialyzed into Tris-buffered saline (TBS) by using PD-10 desalting columns (GE Healthcare), and protein concentrations were measured with a UV-visible spectrophotometer (Pierce). Protein integrity was assessed by UV and CD measurements at the Biomolecular Spectroscopy Centre, King's College London, UK.

On-cell Western™ Blotting—Binding ability of NetB to a chicken hepatocellular carcinoma epithelial cell line (LMH; ATCC: CRL-2117) was addressed by an On-cell Western™ assay using the Odyssey CLx infrared imaging system (Li-Cor). LMH cells were grown in Waymouth's MB 752/1 medium (Invitrogen) supplemented with 10% fetal calf serum at 37 °C in a 5% CO_2 incubator to 70–80% confluency on 96-well plates and fixed with 4% formaldehyde for 20 min at room temperature. After washing three times with TBS, cells were incubated with NetB or TBS only as negative control for 10 min at 37 °C. Cells were then washed 3 times with TBS and blocked by using the Odyssey blocking buffer for 1.5 h at room temperature. Cells were then incubated with an anti-Xpress antibody (Invitrogen; 1:1000) overnight at 4 °C. After washing 3 times with TBS, IRdye 800CW goat anti-mouse (Li-Cor; 1:800) secondary antibody was added, and cells were incubated for 1 h at room temperature. Cells were washed three times with TBS, and fluorescence was measured by the Odyssey CLx infrared scanner.

Cytotoxic Effect of NetB on LMH Cells—The cytotoxicity of NetB on LMH cells was evaluated with the CytoTox96 kit (Promega). LMH cells were grown on 96-well plates as described above and incubated with 2-fold serial dilutions of NetB in Waymouth's medium for 2 h at 37 °C. Control cells were incubated with Waymouth's medium to determine either the base line (0%) or total cell lysis (100%), the latter achieved by freezing and thawing of the cells. Cytotoxicity is shown as percentage relative to the controls.

Hemolysis Assay—Hemolysis assays with NetB were performed using human or chicken red blood cells (hRBCs, cRBCs). At first erythrocytes were washed 3 times with TBS buffer. The final stock suspension was prepared by resuspending RBCs in TBS at 15% (v/v), obtaining a concentration of ~4.6×10^6 cells/ml. A 2-fold dilution series of NetB was made in a 96-well microtiter plate, and RBCs were then added to each well leading to molar concentrations of NetB ranging from 20 nM to 5 μM. The extent of hemolysis was monitored by measuring absorption at 595 nm for 1 h at room temperature with the iMark microplate reader (Bio-Rad) and using the Microplate Manager 6.0 software (Bio-Rad). For selected mutants, additional measurements were taken at 2, 4, and 24 h at a molar concentration of 5 μM. The controls consisted of TBS as the negative control for 0% hemolysis and 2% (v/v) Triton X-100 as the positive control for 100% hemolysis. Data are shown either as the median cytotoxic dose (CT_{50}) for causing 50% hemolysis within 1 h or as the degree of hemolysis after 2, 4, and 24 h compared with the controls.

Liposome Preparation and NetB Oligomer Isolation—To induce oligomerization of NetB, lipid vesicles containing egg phosphatidylcholine, egg phosphatidylglycerol (PG), lysamine-rhodamine B-labeled phosphatidylethanolamine, and cholesterol were prepared. Lipids dissolved in ethanol (Avanti Polar Lipids) were mixed at the appropriate ratio and dried under a nitrogen stream. To ensure no residual solvent remained, lipids were further dried in a vacuum desiccator for 1 h. Lipids were hydrated by the addition of buffer (20 mM Tris, pH 8.0, 150 mM NaCl) and frozen in liquid nitrogen. Lipid suspensions were then thawed at 37 °C, and the freeze-thaw process was repeated two more times. The lipid suspensions were then extruded 21

times through a 100-nm diameter filter using an Avanti lipid extruder. Liposomes were used fresh or frozen at −80 °C until further use. NetB was mixed with liposomes at a protein-to-lipid weight ratio of 2:1 and incubated at 37 °C for 1 h to allow oligomerization. In most cases monomeric NetB was removed by ultracentrifugation at 100,000 × *g* for 45 min at 4 °C using a Beckman TLA 110 rotor. NetB was then extracted in buffer containing 20 mM Tris, pH 7.5, 150 mM NaCl, and detergent (1% (w/v) octyl β-D-glucopyranoside, 5 mM lauryldimethylamine oxide, 40 mM Hexaethylene glycol monodecyl ether (C10E6), or 1 mM pentaethylene glycol monooctyl ether (C8E5)). Unsolubilized material was removed by ultracentrifugation as before. As a final step, detergent-solubilized NetB oligomer was passed over a 25-ml Superose 6 size-exclusion column. During this step the majority of lipid associated with NetB was removed as judged by the color of the fractions; fractions containing solubilized lipid eluted immediately after NetB and were pink in color due to rhodamine-labeled phosphatidylethanolamine. NetB oligomer was then concentrated to 15–18 mg/ml for crystallization using an Amicon 100-kDa cutoff concentrator. The color of the concentrated protein also indicated the presence of some lipids still associated with NetB.

Oligomerization and Calcein Release Assays—Lipid vesicles composed of dioleoylphosphatidylcholine (DOPC), egg PG, and varying amounts of cholesterol were prepared as described above. To measure NetB oligomerization, liposomes (1 mM lipid) or deoxycholic acid (6 or 12 mM) or 2-methyl-2,4-pentanediol (MPD; 10–30% v/v) were mixed with NetB monomer (7 μM) and incubated at 37 °C for 1 h. Samples were then mixed with SDS sample loading buffer and run on 4–12% Bis-Tris SDS-PAGE gels without sample heating or boiling. Gels were Coomassie-stained and digitized using standard procedures. Quantification of monomer reduction was performed using the gel analysis tools in ImageJ (16).

For calcein release experiments, liposomes were prepared using the procedures described above, but lipid films were hydrated using a 75 mM calcein solution in 50 mM Tris, pH 8.0, 150 mM NaCl, and liposomes were separated from excess calcein after extrusion by passage over 15 ml of CL-4B-Sepharose resin. To measure pore formation, NetB was incubated with liposomes of varying lipid composition at 37 °C for 1 h. Calcein release was measured using a FluoroMax-3 fluorometer (Jobin Yvon Horiba) with an excitation and emission wavelength of 495 and 515 nm, respectively. Calcein release (%) was calculated as,

$$\text{Calcein release } \% = (F_{\text{final}} - F_0)/(F_{\text{max}} - F_0) \times 100 \quad \text{(Eq. 1)}$$

where F_{final} is the fluorescence measured after incubation with the toxin, F_0 is the background fluorescence in the absence of toxin, and F_{max} is the fluorescence after addition of 1% (v/v) Triton X-100.

Protein Lipid Overlay Assay—Sphingostrips™ (Echelon Biosciences) were blocked for 1 h at room temperature in TBS-milk (10 mM Tris, pH 8.0, 150 mM NaCl, 1% (w/v) milk). Membranes were then washed three times in TBS, and NetB, *C. perfringens* enterotoxin, or tobacco etch virus protease was added at a final concentration of 5 μg/ml in TBS and left for 16 h at room temperature with gentle shaking. Subsequently membranes were washed 3 times in TBS and incubated with primary anti-His_6 antibodies (GE Healthcare) at a 1:3000 dilution in TBS-milk for 2 h at room temperature. Membranes were washed 3 times again and incubated for 1 h with secondary HRP-conjugated goat anti-mouse antibodies diluted 1:2500 in TBS-milk. Membranes were developed using 4-chloro-1-napthol.

TABLE 1
Data collection and refinement statistics

	Native NetB
Data collection	
Space group	*C2*
Cell dimensions	
a, *b*, *c* (Å)	313.23, 168.04, 160.46
α, β, γ (°)	90, 109.4, 90
Resolution (Å)	27.71-3.9-(4.039-3.9)[a]
R_{merge}	0.344 (0.685)
$I / \sigma I$	3.7 (2.0)
Completeness (%)	97.4 (97.0)
Redundancy	3.7 (3.7)
Refinement	
Resolution (Å)	27.71-3.9
No. reflections	63,875
$R_{\text{work}}/R_{\text{free}}$	28.3/30.8
No. atoms	
Protein	27,960
Ligand/ion	0
Water	0
B-factors, protein	74.40
Root mean square deviation	
Bond lengths (Å)	0.003
Bond angles (°)	0.83

[a] Values in parentheses are for highest resolution shell.

Crystallization and Data Processing—NetB oligomer was crystallized initially using the sitting drop method in 12% (w/v) PEG 4000, 100 mM sodium cacodylate, pH 6.5. However, these crystals were too small for diffraction studies. Optimization using a combination of limited trypsin proteolysis and the addition of the additive detergent polyethylene glycol dodecyl ether (Thesit® part of the Hampton detergent screen) led to crystals that diffracted to ~4 Å. Data were collected on a Rigaku Saturn 944 CCD detector mounted onto a Rigaku Micromax x-ray generator. Data were indexed and integrated with Mosflm (17) and scaled using SCALA (18) as part of the CCP4 (19) package. Molecular replacement was carried out using Phaser MR (20) and the αHL heptamer structure (PDB ID 7AHL) as a search model. The initial model was refined using Phenix (21) with non-crystallographic symmetry, Ramachandran and secondary structure restraints, and increased weighting on stereochemical terms. At the final stages Ramachandran restraints were released. Manual building and real space refinement was performed using COOT (22), and model validation was calculated using Molprobity (23). PyMOL (24) was used for visualization and electrostatic potential surface rendering. A model with all side chains present was used for electrostatic potential calculation even when side-chain density was not visible in the electron density map. Data collection and refinement statistics are shown in Table 1.

RESULTS

Mutations within the Rim Domain of NetB Affect Binding and Toxicity—NetB shares ~30% identity with αHL, the prototypical member of this family of small β-PFTs. Sequence compar-

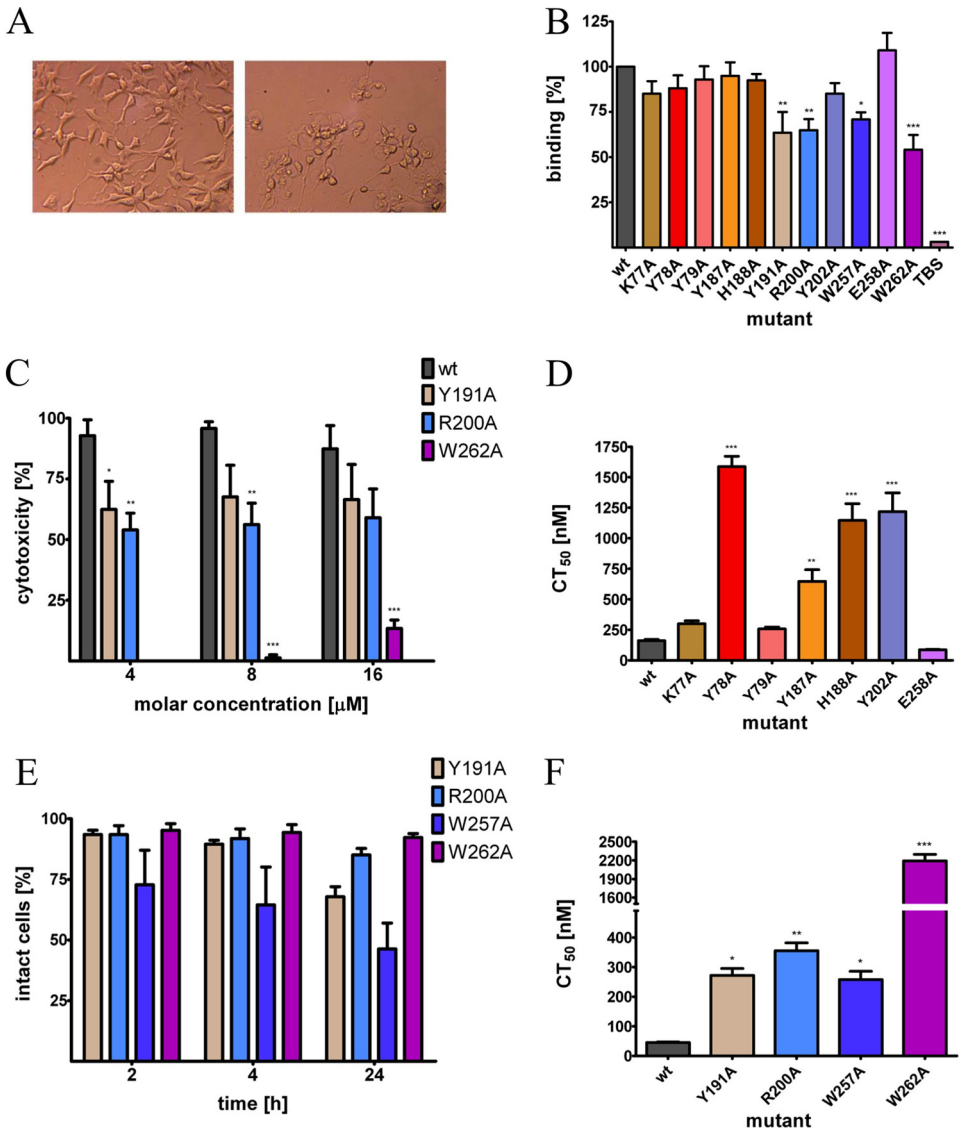

FIGURE 1. **Morphological damage of LMH cells induced by NetB and functional analysis of NetB rim mutants.** *A*, shown are untreated cells (*left panel*) and cells incubated with NetB (800 nM, 1 h, *right panel*). Cell swelling and blebbing induced by NetB can be seen on the *right panel*. *B*, shown is binding to LMH cells. Cells were grown on 96-well plates and incubated with NetB (23 μM) for 10 min at 37 °C. The degree of binding is shown relative to wild type NetB (100%). The graph represents data from four replicates in three independent experiments (data are the means ± S.E.; $n = 3$). *Asterisks* indicate a statistically significant difference (*, $p < 0.05$; **, $p < 0.01$; ***, $p < 0.001$; 1-way analysis of variance) relative to wild type NetB. *C*, shown is the cytotoxic effect of NetB on LMH cells. Cells were grown on 96-well plates and incubated with 2-fold serial dilutions of NetB for 2 h. Cytotoxicity is shown relative to the signal of untreated (0%) and lysed cells (100%). The graph represents data from three replicates in three independent experiments (data are the means ± S.E.; $n = 3$). *Asterisks* indicate a statistically significant difference (*, $p < 0.05$; **, $p < 0.01$; ***, $p < 0.001$; 2-way analysis of variance) relative to wild type NetB. *D—F*, hemolysis of human (hRBCs) or chicken red blood cells (cRBCs) is shown. *D*, a 2-fold dilution series of NetB was incubated with hRBCs for 1 h at 37 °C. The cytotoxic dose to lyse 50% of the cells (CT_{50}) was determined within the given time period. The graph represents data from three independent experiments (data are the means ± S.E.; $n = 3$). *Asterisks* indicate a statistically significant difference (***, $p < 0.001$; **, $p < 0.01$; 1-way analysis of variance) relative to wild type NetB. *E*, rim mutants Y191A, R200A, W257A, and W262A were incubated with hRBCs at a molar concentration of 5 μM, and the degree of hemolysis was determined at 2, 4, and 24 h. Hemolysis is shown relative to the signal of untreated (0%) and lysed (100%) hRBCs. The graph represents data from three independent experiments (data are the means ± S.E.; $n = 3$). *F*, hemolysis of cRBCs was carried out as described for hRBCs and using wild type NetB and mutants Y191A, R200A, W257A and W262A.

isons with other members of this family indicate that a number of residues identified as critical for function among the staphylococcal members are also present in *C. perfringens* NetB, δ and β toxins (supplemental Fig. 1). In this study site-directed mutagenesis was used to determine whether mutation of key residues along the rim loops, assumed to be involved in cell binding, would affect NetB function.

First, NetB was evaluated for cytotoxicity toward LMH cells. The median cytotoxic dose (CT_{50}) of NetB toward LMH cells was determined as 800 nM (supplemental Fig. 2). Fig. 1*A* shows the morphological effects of NetB on LMH cells. The *left panel* demonstrates the epithelial and dendritic-like growth of untreated cells. Treatment with purified NetB (800 nM, 1 h) caused rapid cell blebbing and swelling (*right panel*), whereas longer incubation periods led to total cell lysis. The binding ability of NetB to LMH cells was analyzed using an On-cell Western™ assay. Fig. 1*B* shows binding of each mutant relative to wild type NetB. Mutants Y191A, R200A, W257A, and W262A showed significantly reduced binding compared with wild type toxin, with mutant W262A having the lowest affinity

to the cells. Subsequently, the three NetB mutants showing the lowest affinity in the On-cell Western™ assay (Y191A, R200A, and W262) were tested for their abilities to cause lysis of LMH cells at 4, 8, or 16 μM concentrations (Fig. 1*C*). All three mutants showed reduced cytotoxicity relative to wild type NetB, with W262A showing the highest decrease.

In addition, the hemolytic activity of NetB was evaluated by incubating the toxin with either hRBCs or cRBCs. Fig. 1*D* shows the CT_{50} values of the NetB variants on hRBCs. However, CT_{50} values of mutants Y191A, R200A, W257A, and W262A could not be determined, as they only caused incomplete hemolysis within 1 h, even at 5 μM concentrations. Therefore, these mutants were incubated with hRBCs for an extended period, and the degree of hemolysis was monitored at 2, 4, and 24 h (Fig. 1*E*). Again, mutants Y191A, R200A, W257A, and W262A showed the most significant decrease in activity relative to wild type NetB. In addition, mutants Y78A, Y187A, H188A, and Y202A also showed a significant increase in CT_{50} values. When cRBCs were tested for hemolysis, the CT_{50} value of the wild type was more than 3-fold lower as compared with hRBCs (Fig. 1*F*). Furthermore, the CT_{50} of the mutants Y191A, R200A, W257A, and W262A could now be measured as they caused complete hemolysis within the 1-h time frame. However, their activity was significantly lower than of wild type toxin.

In summary, replacement of conserved residues along the rim loops of NetB (Tyr-191, Arg-200, Trp-257, and Trp-262) had the most dramatic effect on NetB cell binding and toxicity. In addition, due to the broader dynamic range of the hemolysis assay, it could be shown that non-conserved residues such as Tyr-78, Tyr-187, His-188, and Tyr-202 also play a role in NetB function.

NetB Oligomerizes and Forms Discrete Pores on Cholesterol-rich Vesicles—NetB is secreted as a water-soluble monomer that is thought to oligomerize on the target cell surface before pore formation (11). When overexpressed in *Escherichia coli*, NetB accumulates in the cytoplasm in its monomeric form and can be purified by standard metal-affinity chromatography. To promote assembly of the oligomer, we tested the effect of detergents, amphiphiles, and lipids on the oligomeric state of NetB. The addition of the ionic detergent deoxycholate above the critical micelle concentration (6 or 12 mM) or MPD (10–30% v/v) did not produce SDS-resistant oligomers (Fig. 2*A*). However, the presence of 20–30% (v/v) MPD did affect NetB, evidenced by the reduction of the monomer and a smeary appearance in these lanes (Fig. 2*A*, *lanes 2* and *3*). MPD may cause NetB to form aggregates that cannot enter the gel. These findings are in contrast to αHL, which assembles into the membrane-inserted form upon the addition of deoxycholate (25) or MPD above 20% (v/v) (26). Next, liposomes composed of the pure, unsaturated lipid DOPC, egg PG, and cholesterol were evaluated for their ability to promote NetB oligomerization. The efficiency of oligomerization was assessed by incubating NetB and liposomes at a molar ratio of 350:1 (NetB:liposomes) and monitoring the reduction of monomer on SDS-PAGE. In the absence of cholesterol, 85% of the total protein was in the monomeric form, indicating that NetB had only partially oligomerized (Fig. 2*B*, *lane 2*). The monomer fraction decreased to 65, 35, and 10% of the total protein input in the presence of 0.1, 0.2, and 0.5 molar ratio of cholesterol, respectively (Fig. 2*B*, *lanes 3–5*). The decrease of monomer was also accompanied by a corresponding increase of SDS-resistant oligomers. Thus, the inclusion of cholesterol promoted NetB oligomerization with an almost linear dependence.

To further investigate the role of cholesterol and to test if oligomerization of NetB corresponds to the formation of productive pores, we used small unilamellar vesicles loaded with the self-quenching fluorophore calcein (R_H = 8 Å (27)). Liposomes were subjected to increasing amounts of NetB monomer and incubated at 37 °C for 1 h. The total fluorescence was then measured as an indicator of calcein release (pore formation) and normalized against 100% calcein release using Triton X-100. As seen in Fig. 2*C*, vesicles without cholesterol promoted pore formation by NetB only at high protein concentrations and resulted in ~30% calcein release. However, the inclusion of cholesterol increased pore formation in a dose-dependent way. For example, vesicles with 50 mol% cholesterol allowed 10 times more calcein release than vesicles with 10 mol% cholesterol (at 1 μM NetB). Cone-shaped lipids such as cholesterol promote the transition of the bilayer to the inverted hexagonal phase, which may facilitate toxin insertion (28). To investigate whether the shape of the phospholipids is important for NetB insertion, vesicles containing 50 mol% egg phosphatidylethanolamine, also a cone-shaped lipid, were tested for pore formation. As seen in Fig. 2*C*, these vesicles did not readily promote pore formation.

We reasoned that the effect of cholesterol on NetB activity might be due to a better exposure of the phosphocholine head groups of DOPC, which may act as a receptor for the toxin. This would concentrate the toxin on the membrane surface, allowing it to oligomerize and insert more efficiently as reported previously for αHL (29). To determine if NetB can bind to a specific lipid moiety, we performed a simple protein lipid overlay assay. Membranes spotted with 100 pmol of various lipids (Sphingostrips™) were incubated with NetB bearing an N-terminal hexahistidine tag, and binding specificity was probed using anti-His_6 antibodies. Surprisingly, NetB bound to cholesterol but not to phosphatidylcholine (Fig. 2*D*). Some binding was also seen to the glycosphingolipid sulfatide but to a lesser extent. No binding of NetB was observed to sphingomyelin. Negative controls using *C. perfringens* enterotoxin (Fig. 2*E*) and tobacco etch virus protease (Fig. 2*F*) revealed no binding to cholesterol but some binding to sulfatide, as seen for NetB.

To confirm that NetB formed discrete pores and that calcein was not being released as a result of liposome fragmentation, NetB-liposome mixtures were observed by transmission electron microscopy. Negatively stained specimens showed ring-shaped structures protruding from the liposomes, which measured ~10 nm in diameter (Fig. 2*G*). Furthermore, the liposome size distribution seemed unaffected by NetB as compared with lipid only controls (supplemental Fig. 3). Collectively, these results indicate that NetB produces discrete pores of at least 1.6 nm in diameter, and although NetB is able to oligomerize and form pores in the presence of phosphatidylcholine vesicles alone, at lower NetB concentrations inclusion of cholesterol increases the conversion to oligomer and pore formation by almost an order of magnitude. Finally the lipid overlay assay

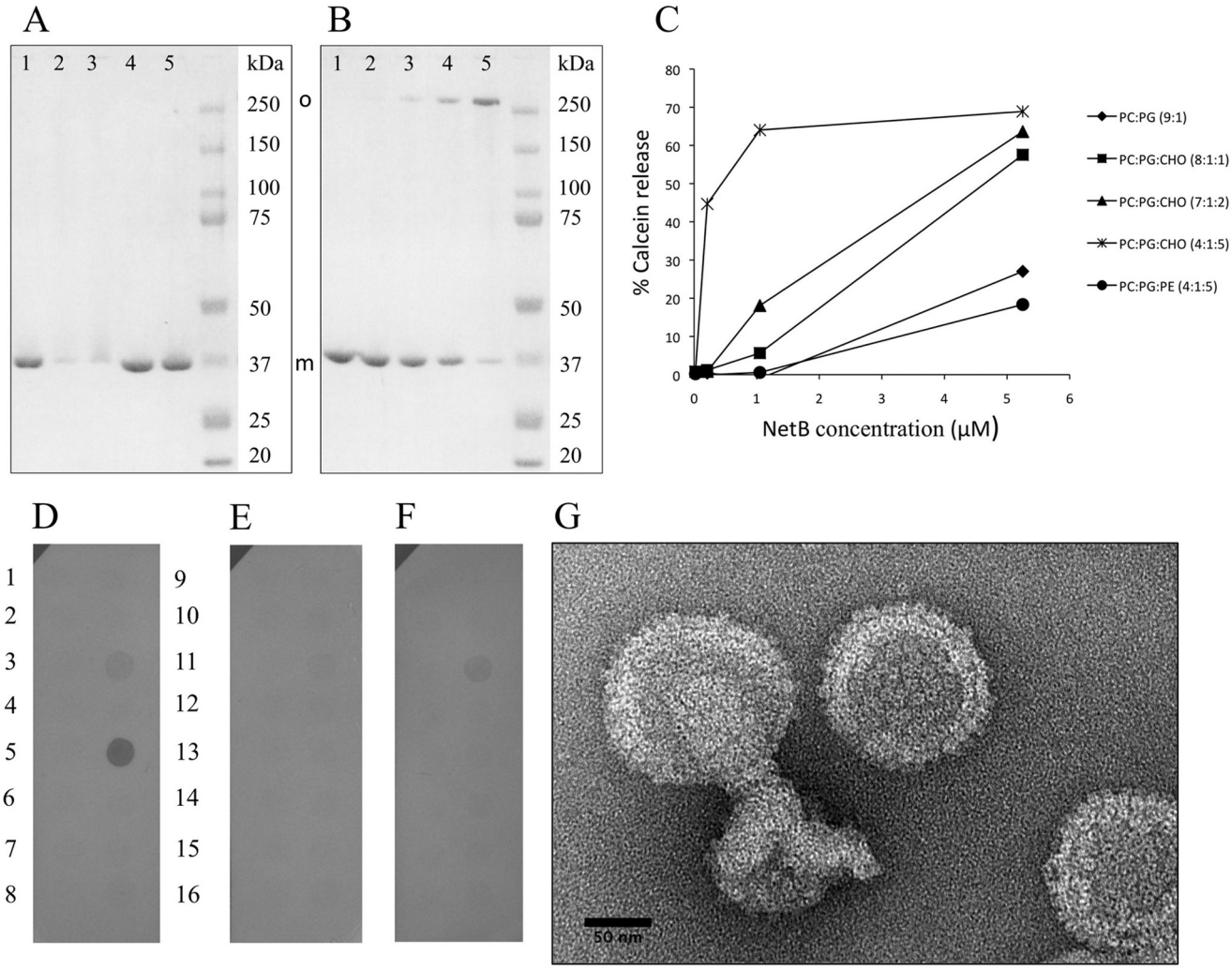

FIGURE 2. ***In vitro* oligomerization and pore-forming activity of NetB.** *A*, NetB oligomerization in the presence of amphiphiles is shown. Monomer and oligomer band positions are indicated. *Lane 1*, NetB plus 10% (v/v) MPD. *Lane 2*, NetB plus 20% (v/v) MPD. *Lane 3*, NetB plus 30% (v/v) MPD. *Lane 4*, NetB plus 6 mM deoxycholate. *Lane 5*, NetB plus 12 mM deoxycholate. *B*, NetB oligomerization in the presence of liposomes is shown. *Lane 1*, NetB only. *Lane 2*, NetB plus DPOC:PG (9:1). *Lane 3*, NetB plus DPOC:PG:Cho (8:1:1). *Lane 4*, NetB plus DPOC:PG:Cho (7:1:2). *Lane 5*, NetB plus DPOC:PG:Cho (4:1:5). SDS-PAGE samples were run without boiling. *Cho*, cholesterol. *PE*, phosphatidylethanolamine. *C*, calcein-loaded liposomes of the indicated compositions were incubated with NetB at various concentrations for 1 h at 37 °C, and the % calcein release was measured. *D–F*, shown are protein lipid overlay assays with NetB (*D*), *C. perfringens* enterotoxin (*E*), and tobacco etch virus protease (*F*). SphingoStrips™ (Echelon) were incubated with the His_6-tagged proteins as described under "Experimental Procedures" and developed using ani-His_6 antibodies. Lipid spots: *1*, sphingosine; *2*, sphingosine-1-phosphate; *3*, phytosphingosine; *4*, ceramide; *5*, sphingomyelin; *6*, sphingosylphosphorylcholine; *7*, lysophosphatic acid; *8*, myriosin; *9*, monosialoganglioside; *10*, disialoganglioside; *11*, 3-sulfogalactoceramide (sulfatide); *12*, psychosine; *13*, cholesterol; *14*, lysophosphocholine; *15*, phosphatidylcholine; *16*, blank. *G*, electron microscopy of NetB-liposome mixtures is shown. NetB were mixed with liposomes containing cholesterol (50 mol %). Samples were negatively stained with 2% (w/v) aqueous uranyl acetate and observed using a Philips T12 transmission electron microscope. The liposomes appear completely decorated with 10-nm ring structures, whereas some side views are visible at the liposome edges extending above the liposome surface.

clearly shows that NetB is able to bind directly to cholesterol in the absence of any other lipids.

Solubilization and Crystallization of the NetB Oligomer—A range of non-ionic and zwitterionic detergents were tested for their abilities to solubilize and maintain the oligomers of NetB, which were observed in lipid vesicles, in micellar solution. Lauryldimethylamine-oxide, octyl β-D-glucopyranoside, and hexaethylene glycol monodecyl ether (C10E6) efficiently solubilized the NetB assemblies, indicated by a sharp oligomer peak on size-exclusion chromatography (supplemental Fig. 4). In contrast, the detergent pentaethylene glycol monooctyl ether (C8E5) resulted in a broad elution profile and led to NetB precipitation immediately after elution. Interestingly, residual lipids from the liposomes were still associated with NetB even after size-exclusion chromatography (see "Experimental Procedures"). Detergents that efficiently solubilized NetB were then used for crystallization trials. Only NetB solubilized in C10E6 yielded crystals that diffracted beyond 12 Å. Crystal quality was improved by the addition of an additive detergent and limited proteolysis using trypsin, which resulted in the removal of the first 20 residues from the N terminus as determined by N-terminal sequencing. The best crystals belonged to the space group *C2* (unit cell dimensions; $a = 313$ Å, $b = 168$ Å, $c = 160$ Å, $\alpha = 90°$, $\beta = 109.4°$, $\gamma = 90°$) and diffracted to ~4 Å. Molecular replacement using the αHL heptamer (PDB ID 7AHL) resulted in a single solution with two heptamers in the asymmetric unit and a solvent content of 71%. The presence of 14-fold non-crystallographic symmetry (NCS) produced maps

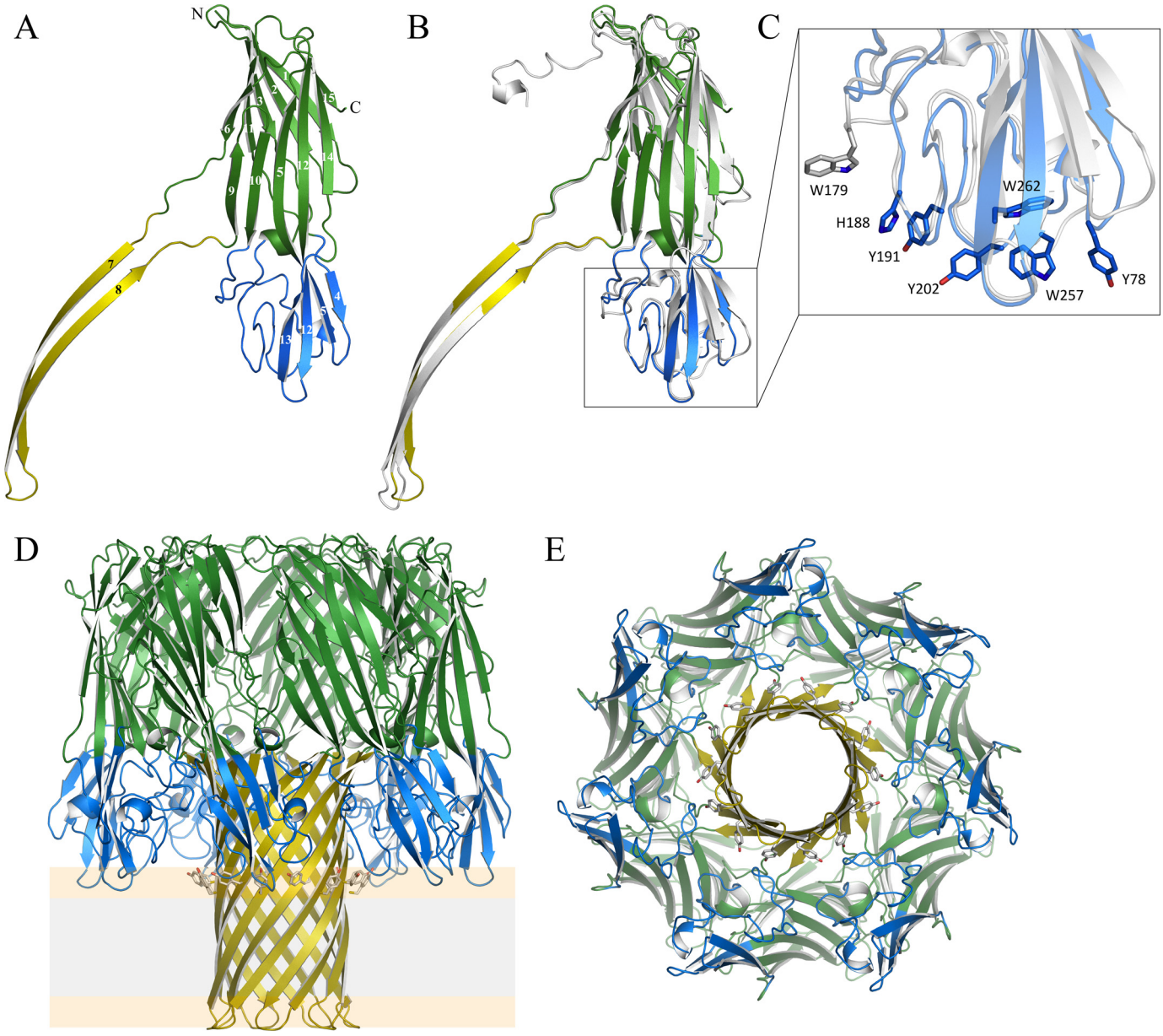

FIGURE 3. **Crystal structure of NetB.** *A*, shown is a ribbon representation of an isolated NetB subunit. The three domains are colored *green* (β-sandwich domain), *blue* (rim domain), and *yellow* (stem domain), and β-strands are numbered as described in "Results." The N and C termini are indicated. *B*, superposition of a NetB subunit to an αHL subunit (*light gray*) indicates the overall similarities and differences between the two proteins. *C*, shown is a close-up view of the rim domain. Residues in NetB that were mutated in this study and shown to affect function are shown in *stick representation*. *D* and *E*, shown is a ribbon representation of the NetB assembly (colored as in *A*) viewed from the side (*D*) and cytoplasmic aspects (*E*). Residues Tyr-123 and Tyr-144, which form an aromatic belt on the stem, are shown in *stick representation*. The putative borders of the membrane bilayer are indicated with the phospholipid head groups of both leaflets in *yellow* and the hydrophobic core in *gray*.

in which most of the protein chain could be built and the side chains could be placed with an accuracy that is unusually high for this resolution (supplemental Fig. 5). Although trypsin removed the first 20 residues, electron density was only visible from residue 25.

Structure of NetB and Pore Assembly—Each NetB monomer contains 15 β-strands, accounting for 53% of the polypeptide, whereas the remainder is made up of one 3_{10}-helix, one short α-helix, and random coil. As with αHL (12), NetB can be divided into three main domains: β-sandwich, rim, and stem (Fig. 3*A*). The β-sandwich domain consists of two β-sheets composed of strands 1, 2, 3, 6, and 11 and strands 5, 9, 10, 12, 14, and 15, and a single α-helix. Strands 5 and 12 extend into the lower part of the molecule, and these strands along with strands 4 and 13, the 3_{10} -helix and considerable random coil, make up the rim domain. The stem domain contains the long, curved amphipathic hairpin (strands 7 and 8), which is connected to the β-sandwich domain through two short coils, forming a triangle region similar to that in other membrane-inserted β-PFTs (12, 13). As described above, the first 20 N-terminal residues were removed by trypsin, and therefore, the amino-latch equivalent region, which latches on to the adjacent subunit in αHL (12), is not present in the NetB structure. A NetB monomer shares the highest structural similarity with δ toxin

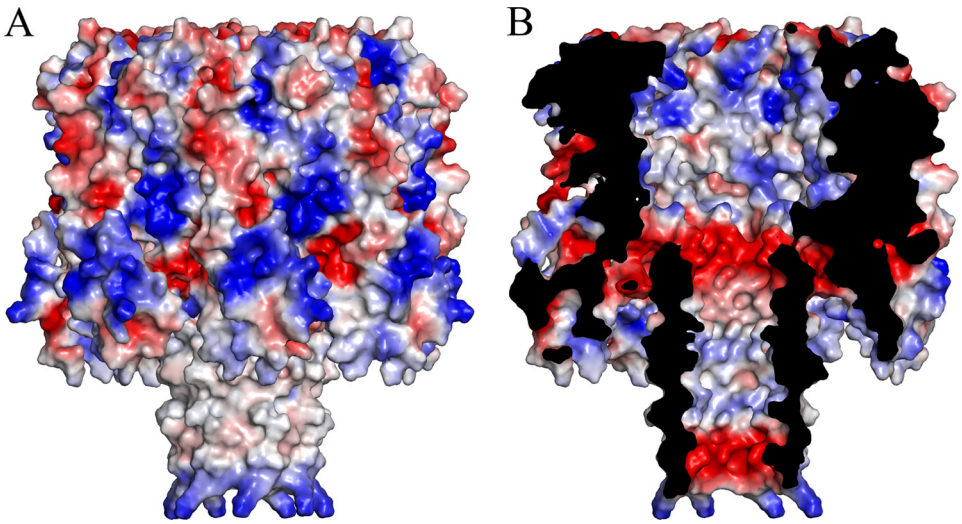

FIGURE 4. **Surface charge distribution in NetB.** Surface electrostatic potential calculated using the PyMOL molecular graphics program shows the exterior of the NetB heptamer (*A*) and a cut-out view revealing the channel's interior surface (*B*). *White*, neutral; *blue*, positive charge; *red*, negative charge.

from *C. perfringens* (PDB ID 2YGT). Superposition of a NetB monomer with δ toxin results in a root mean square deviation of 1.2 Å (Cα-Cα) by secondary structure matching (19) even though the δ toxin structure represents the water-soluble monomer without the stem extended. Superposition with the *S. aureus* αHL monomer results in a root mean square deviation of 1.55 Å. Fig. 3*B* illustrates the structural conservation between NetB and αHL. With the exception of two small β-strands that are absent in NetB (αHL strands 11 and 12; supplemental Fig. 1), secondary structure elements are largely conserved between the two toxins. Areas of small structural deviation to αHL exist in all three domains. For example, loop positions in the β-sandwich domain between strands 5 and 6 and strands 11 and 12 deviate from the corresponding loops in αHL. Strand 15 in αHL, which spans the rim and β-sandwich domains, is composed of two separate strands (13 and 14) in NetB. Finally, although the NetB stem domain adopts a similar curvature to αHL, the turn at the cytoplasmic end bends inward toward the pore lumen in NetB.

The most interesting differences between the two toxins lie in the area that constitutes the rim loops (Fig. 3*C*). In particular, a loop after strand 10 (Val-176—Ile-184) is shorter than that of αHL (Asn-172—Arg-184) and does not contain an equivalent to Trp-179, a residue important for lipid binding in αHL and LukF (Trp-177) (12, 30, 31). In addition, strand 4 in NetB lies ~6 Å closer to the 7-fold axis, accounting for a smaller heptamer diameter compared with the αHL heptamer (see below).

A NetB oligomer is composed of seven monomers arranged in a ring that measures 90 Å in diameter and 95 Å along the 7-fold non-crystallographic symmetry axis (Fig. 3, *D* and *E*). Thus, the NetB heptamer is slightly more compact than the αHL (100 × 100 Å) (12), γHL (114 × 93 Å) (13), and VCC (135 × 140 Å) (14) assemblies. Each monomer buries a total surface area of ~4200 Å^2 and forms an extensive hydrogen bond network and a number of salt bridges on both interfaces, including Lys-41 (positional equivalent to His-35 in αHL), which forms a salt bridge to Asp-164 of the neighboring molecule. The seven β-sandwich domains form the cap of the mushroom-shaped heptamer, whereas the stem domains form the 14-strand β-barrel pore. Each β-hairpin extends from Lys-114 and ends at Pro-155, with a GKT tripeptide forming a turn at the cytoplasmic side of the pore. The amphipathic composition of the β-hairpin is illustrated in supplemental Fig. 1. The predicted transmembrane region spans Ile-121 to Val-146 with Ile, Tyr, Val, Ala, and Gly residues exposed to the bilayer, whereas the lumen of the pore consists of uncharged polar residues, glycines, and a single charged residue, Glu-132, at the cytoplasmic entrance of the pore. Two aromatic residues, Tyr-123 on strand 7 and Tyr-144 on strand 8, form an aromatic belt at the upper side of the pore, similar to VCC (14) and some outer membrane proteins (32), and could reside at the hydrophobic core-polar head group interface of the outer bilayer leaflet. The distance from the cytoplasmic entrance of the pore to the aromatic belt is ~27 Å and ~35 Å to the predicted start of the trans-membrane region. A surface representation of the pore colored by electrostatic potential, as calculated by PyMOL (24), exemplifies the hydrophobic nature of the transmembrane region (Fig. 4*A*). Examination of the charge distribution in the pore lumen reveals two distinct negatively charged areas on either entrance of the β-barrel pore (Fig. 4*B*). The extracellular side is lined by Asp116 and Glu-153, whereas Glu-132 lines the cytoplasmic entrance. The two negatively charged areas in the NetB pore might influence the selectivity of ions across the membrane. The pore measures ~26 Å in diameter (Cα-Cα), similar to the pores of other members of this family (12–14).

DISCUSSION

Necrotic enteritis is an emerging infectious disease in poultry causing huge economic losses to the livestock industry worldwide. NetB, a novel toxin produced by *C. perfringens*, appears to play a key role in the disease. Here, we present the crystal structure of the oligomeric form of NetB, which to our knowledge is the first near-atomic resolution structure of a clostridial β-PFT in the pore state. The heptameric structure, which displays high structural similarity to the staphylococcal toxin αHL, reveals conservation of many of the key residues that are important for

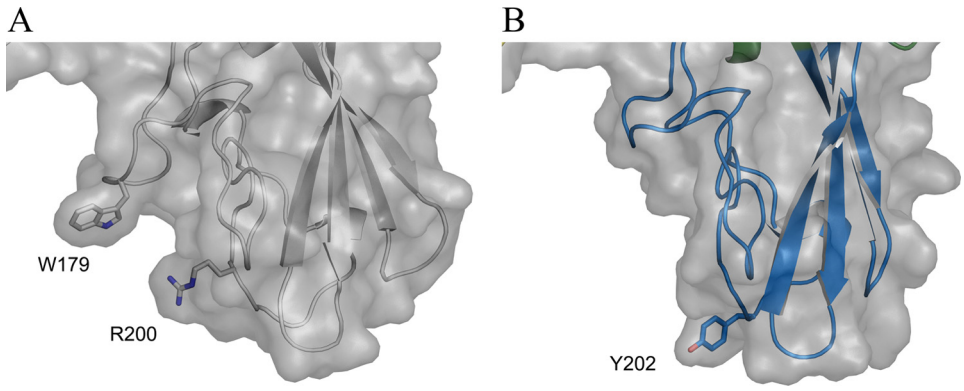

FIGURE 5. **Phospholipid binding at the rim domain.** Surface representation is shown of the rim domain of αHL (PDB ID 7AHL) (*A*) and NetB (*B*) in the same orientation. The phosphocholine binding pocket, which is formed by Trp-179 and Arg-200 in αHL, is absent in NetB. Tyrosine 202 in NetB affects binding and toxicity and could be involved directly in lipid binding. Arginine 200 in NetB is disordered and thus absent from the model.

function in this family of β-PFTs but displays differences that may have evolved separately in the clostridial counterparts.

Binding to the membrane surface of the target cell in this family of PFTs is mediated through the rim domain. This domain contains loops rich in aromatic residues that are proposed to interact with the outer leaflet of the bilayer, and in the case of VCC, these loops may extend further into the membrane and help to destabilize it (14). Residues Trp-179 and Arg-200 in αHL (equivalent to Trp-177 and Arg-198 in LukF), which are located within the rim loops, are essential for toxin function (33, 34) and form a phospholipid binding pocket (Fig. 5*A*) that has been captured interacting with phosphatidylcholine analogues and amphiphilic groups in several crystallographic structures (12, 13, 26, 30, 31). High resolution crystallographic studies of αHL in complex with glycerophosphocholine showed that Arg-200 forms a water-mediated hydrogen bond to the phosphate, whereas Trp-179 contacts the quaternary ammonium group through cation-π interactions (30). In NetB, mutation of Arg-200 to alanine leads to a significant reduction of binding and toxicity, confirming the importance of this residue in host cell interactions. However, a Trp-179 equivalent is not present in NetB or in the other clostridial toxins (supplemental Fig. 1), and the equivalent rim loop in NetB is shorter. Therefore, this lipid binding residue and consequently the phosphocholine binding pocket is lost in NetB (Fig. 5*B*). This suggests that NetB and possibly the other clostridial toxins may bind to the host membrane through alternative interactions. In support of this hypothesis are three lines of evidence. First, the protein lipid overlay assay and the calcein release experiments indicate that NetB does not interact efficiently with phosphatidylcholine or sphingomyelin, both of which have phosphocholine head groups. Second, the same assays indicate that NetB interacts directly with cholesterol, and pore formation is enhanced by its presence in bilayers. Third, the monomeric form of δ toxin from *C. perfringens*, which is closely related to NetB and has specificity for ganglioside GM2, has recently been crystallized in the presence of glycerol that mimics the phospholipid groups (PDB ID 2YGT). One of the glycerol molecules forms hydrogen bonds with residues 199–202, including Arg-200, whereas Tyr-201 interacts with the glycerol backbone. In NetB, Tyr-202 may facilitate a similar interaction due to its proximity to Arg-200, and this would explain the reduced hemolytic activity of NetB Y202A (Fig. 1*D*). Interestingly tyrosines at this position are only conserved in the clostridial toxins. Thus the clostridial and staphylococcal members of this family of β-PFTs may bind to host membranes using different mechanisms and involving interactions with different lipids.

Tyrosine at position 191 is conserved across this toxin family and in its equivalent substitution in *C. perfringens* β toxin (Y203F) increases the median lethal dose in mice by more than 2-fold (35). This study has shown that residue Tyr-191 affects host cell binding and consequently cytotoxicity of NetB. A reduction in membrane binding may explain the reduced toxicity of β toxin mutant Y203F. On the neighboring rim loop that extends the farthest toward the membrane, Trp-257 and Trp-262 are also involved in cell binding. Substitution to alanine at either position severely reduces NetB binding to LMH cells, significantly reduces hemolysis on cRBCs, and almost abolishes hemolysis on hRBCs (Fig. 2). These residues are highly conserved in β-PFTs of *S. aureus* and *C. perfringens*, and in LukF, W257A abolishes binding to hRBC (33).

The role of the lipid bilayer composition in the function of pore-forming toxins has been extensively studied (28, 36–39). Cholesterol modulates the fluidity of lipid bilayers and promotes a liquid-ordered state intermediate between the gel and liquid-crystalline states at temperatures below the specific transition temperature (T_m) of the lipid (40). This property has been implicated in the function of αHL (37). It has also been suggested that cholesterol may allow the optimal orientation of phosphocholine head groups for toxin interaction (29, 36). Valeva *et al.* (29) suggested that clustering of phosphocholine head groups in cholesterol-sphingomyelin-containing lipid rafts may act as a high affinity receptor for αHL by exposing more of the phosphocholine head groups. The same study showed that cholesterol depletion of rabbit erythrocytes significantly reduced the sensitivity to αHL, and this was attributed to the disruption of clustered sphingomyelin in lipid rafts (29). It was also hypothesized that cholesterol may interact directly with αHL (36) even though it is not a cholesterol-dependent cytolysin. Moreover, cholesterol, which has a similar overall structure to deoxycholate, a detergent that induces oligomerization of αHL, may facilitate the conformational changes that occur during the insertion process (26). In the case of γHL it was shown that toxin function was not affected by membrane fluidity but

was influenced by the physical properties of the phospholipid (shape and length) and the presence of cholesterol (38). As shown here, NetB activity is also influenced by cholesterol. Liposomes composed of 90 mol% DOPC and no cholesterol did not readily induce oligomerization of NetB, and calcein release occurred only at higher protein concentration. Vesicles composed mostly of DOPC (T_m = −20 °C) should exist in the liquid-crystalline state at the experimental temperatures (>23 °C). Thus, membrane fluidity is not the sole factor affecting NetB pore formation. The inclusion of cholesterol up to 50 mol% enhanced oligomerization and calcein release by almost 10-fold. In addition, we showed that it is not the conical shape of cholesterol that confers the bilayer susceptibility to NetB. Finally we show that NetB is able to interact with cholesterol directly in the absence of other lipids. These potentiating properties of cholesterol may reflect a toxin-receptor interaction. At high NetB concentrations, enough monomers may be in close proximity that even weak and transient toxin-membrane interactions may suffice to promote oligomerization. However, at low protein concentrations, stronger interactions for toxin binding are required and may be provided by cholesterol directly. Therefore, although NetB does not belong to the classical cholesterol-dependent cytolysin family, like VCC, its activity is dependent on cholesterol. Although the exact role of membrane cholesterol in NetB function needs to be investigated further, it is clear from this study that it plays a key role in the ability of the toxin to oligomerize and form functional pores. These results may reflect the differences in affinity to target cells *in vivo* and suggest that the different susceptibility of cells to this family of toxins may be attributed to the composition of the cytoplasmic membrane in addition to a putative protein receptor.

Charged residues in the proximity of the pore entrance and along the pore lumen can affect the ion selectivity and function of this family of β-PFTs (41–43), and much effort has been placed in altering the physicochemical properties of these channels for use in nanotechnology (44, 45). In αHL, the cytoplasmic entrance contains two aspartates (Asp-127 and Asp-128), both of which form salt bridges with Lys-131 of the neighboring molecule (12). In addition, Glu-111 on the extracellular side of the αHL pore is involved in a salt bridge with Lys-147. Thus, the overall charge of the αHL pore is neutral with a slight anion selectivity, which is attributed to Lys-147 lying closer to the lumen center than Glu-111 (43). In γHL (HlgA-HlgB) the removal of a single positive charge in the pore lumen (HlgA Lys-108) significantly increases the conductance and cation selectivity of the channel (41). The entrances from both sides of the NetB pore are lined with acidic residues (Asp-116, Glu-153, and Glu-132) forming two distinct negatively charged belts (Fig. 4*B*). Given the influence of charged residues on ion selectivity and the absence of any compensating positive charges, we expect the NetB pore to be cation-selective.

In conclusion, the structure of NetB along with the identification of residues important for binding and toxicity will facilitate the development of vaccines against necrotic enteritis as well as provide the framework for future studies on this group of related pore-forming toxins. Finally, NetB could provide a new set of tools for the field of nanotechnology that will benefit greatly by the availability of a molecular structure in the active form.

Acknowledgments—We are grateful to Dr. Alice Clark and Dr. Natalya Lukoyanova for useful suggestions and advice and to Dr. Tina Daviter (ISMB biophysics center) for assistance and suggestions.

REFERENCES

1. Schwarz, S., Kehrenberg, C., and Walsh, T. R. (2001) Use of antimicrobial agents in veterinary medicine and food animal production. *Int. J. Antimicrob. Agents* **17,** 431–437
2. Anonymous (2001) *WHO Global Strategy for Containment of Antimicrobial Resistance*, World Health Organization, Geneva
3. Kaldhusdal, M., and Hofshagen, M. (1992) Barley inclusion and avoparcin supplementation in broiler diets. 2. Clinical, pathological, and bacteriological findings in a mild form of necrotic enteritis. *Poult. Sci.* **71,** 1145–1153
4. Brennan, J., Moore, G., Poe, S. E., Zimmermann, A., Vessie, G., Barnum, D. A., and Wilson, J. (2001) Efficacy of in-feed tylosin phosphate for the treatment of necrotic enteritis in broiler chickens. *Poult. Sci.* **80,** 1451–1454
5. Brennan, J., Bagg, R., Barnum, D., Wilson, J., and Dick, P. (2001) Efficacy of narasin in the prevention of necrotic enteritis in broiler chickens. *Avian Dis.* **45,** 210–214
6. Elwinger, K., Schneitz, C., Berndtson, E., Fossum, O., Teglöf, B., and Engström, B. (1992) Factors affecting the incidence of necrotic enteritis, caecal carriage of *Clostridium perfringens*, and bird performance in broiler chicks. *Acta Vet. Scand.* **33,** 369–378
7. Kaldhusdal, M., Schneitz, C., Hofshagen, M., and Skjerve, E. (2001) Reduced incidence of *Clostridium perfringens*-associated lesions and improved performance in broiler chickens treated with normal intestinal bacteria from adult fowl. *Avian Dis.* **45,** 149–156
8. Dahiya, J. P., Wilkie, D. C., Van Kessel, A. G., and Drew, M. D. (2006) Potential strategies for controlling necrotic enteritis in broiler chickens in post-antibiotic era. *Animal Feed Science and Technology* **129,** 60–88
9. Van Der Sluis, W. (2000) Clostridial enteritis is an often underestimated problem. *World Poultry* **16,** 42–43
10. Van Der Sluis, W. (2000) Clostridial enteritis. A syndrome emerging worldwide. *World Poultry* **16,** 56–57
11. Keyburn, A. L., Boyce, J. D., Vaz, P., Bannam, T. L., Ford, M. E., Parker, D., Di Rubbo, A., Rood, J. I., and Moore, R. J. (2008) NetB, a new toxin that is associated with avian necrotic enteritis caused by *Clostridium perfringens*. *PLoS Pathog.* **4,** e26
12. Song, L., Hobaugh, M. R., Shustak, C., Cheley, S., Bayley, H., and Gouaux, J. E. (1996) Structure of staphylococcal α-hemolysin, a heptameric transmembrane pore. *Science* **274,** 1859–1866
13. Yamashita, K., Kawai, Y., Tanaka, Y., Hirano, N., Kaneko, J., Tomita, N., Ohta, M., Kamio, Y., Yao, M., and Tanaka, I. (2011) Crystal structure of the octameric pore of staphylococcal γ-hemolysin reveals the β-barrel pore formation mechanism by two components. *Proc. Natl. Acad. Sci. U.S.A.* **108,** 17314–17319
14. De, S., and Olson, R. (2011) Crystal structure of the *Vibrio cholerae* cytolysin heptamer reveals common features among disparate pore-forming toxins. *Proc. Natl. Acad. Sci. U.S.A.* **108,** 7385–7390
15. Gholamiandekhordi, A. R., Ducatelle, R., Heyndrickx, M., Haesebrouck, F., and Van Immerseel, F. (2006) Molecular and phenotypical characterization of *Clostridium perfringens* isolates from poultry flocks with different disease status. *Vet Microbiol* **113,** 143–152
16. Schneider, C. A., Rasband, W. S., and Eliceiri, K. W. (2012) NIH Image to ImageJ. 25 years of image analysis. *Nat. Methods* **9,** 671–675
17. Battye, T. G., Kontogiannis, L., Johnson, O., Powell, H. R., and Leslie, A. G. (2011) iMOSFLM. A new graphical interface for diffraction-image processing with MOSFLM. *Acta Crystallogr. D Biol. Crystallogr.* **67,** 271–281
18. Evans, P. (2006) Scaling and assessment of data quality. *Acta Crystallogr. D. Biol. Crystallogr.* **62,** 72–82
19. Winn, M. D., Ballard, C. C., Cowtan, K. D., Dodson, E. J., Emsley, P., Evans, P. R., Keegan, R. M., Krissinel, E. B., Leslie, A. G., McCoy, A., McNicholas,

S. J., Murshudov, G. N., Pannu, N. S., Potterton, E. A., Powell, H. R., Read, R. J., Vagin, A., and Wilson, K. S. (2011) Overview of the CCP4 suite and current developments. *Acta Crystallogr. D. Biol. Crystallogr.* **67,** 235–242
20. McCoy, A. J., Grosse-Kunstleve, R. W., Adams, P. D., Winn, M. D., Storoni, L. C., and Read, R. J. (2007) Phaser crystallographic software. *J. Appl. Crystallogr.* **40,** 658–674
21. Adams, P. D., Afonine, P. V., Bunkóczi, G., Chen, V. B., Davis, I. W., Echols, N., Headd, J. J., Hung, L. W., Kapral, G. J., Grosse-Kunstleve, R. W., McCoy, A. J., Moriarty, N. W., Oeffner, R., Read, R. J., Richardson, D. C., Richardson, J. S., Terwilliger, T. C., and Zwart, P. H. (2010) PHENIX. A comprehensive Python-based system for macromolecular structure solution. *Acta Crystallogr. D. Biol. Crystallogr.* **66,** 213–221
22. Emsley, P., Lohkamp, B., Scott, W. G., and Cowtan, K. (2010) Features and development of Coot. *Acta Crystallogr. D. Biol. Crystallogr.* **66,** 486–501
23. Davis, I. W., Leaver-Fay, A., Chen, V. B., Block, J. N., Kapral, G. J., Wang, X., Murray, L. W., Arendall, W. B., 3rd, Snoeyink, J., Richardson, J. S., and Richardson, D. C. (2007) MolProbity. All-atom contacts and structure validation for proteins and nucleic acids. *Nucleic Acids Res.* **35,** W375–W383
24. DeLano, W. L. (2010) *The PyMOL Molecular Graphics System*, Version 1.3r1, Schrodinger, LLC, New York
25. Bhakdi, S., Füssle, R., and Tranum-Jensen, J. (1981) Staphylococcal α-toxin. Oligomerization of hydrophilic monomers to form amphiphilic hexamers induced through contact with deoxycholate detergent micelles. *Proc. Natl. Acad. Sci. U.S.A.* **78,** 5475–5479
26. Tanaka, Y., Hirano, N., Kaneko, J., Kamio, Y., Yao, M., and Tanaka, I. (2011) 2-Methyl-2,4-pentanediol induces spontaneous assembly of staphylococcal α-hemolysin into heptameric pore structure. *Protein Sci.* **20,** 448–456
27. Edwards, D. E., Prausnitz, M. R., Langer, R., and Weaver, J. C. (1995) Analysis of enhanced transdermal transport by skin electroporation. *J. Control Release* **34,** 211–221
28. Alonso, A., Goñi, F. M., and Buckley, J. T. (2000) Lipids favoring inverted phase enhance the ability of aerolysin to permeabilize liposome bilayers. *Biochemistry* **39,** 14019–14024
29. Valeva, A., Hellmann, N., Walev, I., Strand, D., Plate, M., Boukhallouk, F., Brack, A., Hanada, K., Decker, H., and Bhakdi, S. (2006) Evidence that clustered phosphocholine head groups serve as sites for binding and assembly of an oligomeric protein pore. *J. Biol. Chem.* **281,** 26014–26021
30. Galdiero, S., and Gouaux, E. (2004) High resolution crystallographic studies of α-hemolysin-phospholipid complexes define heptamer-lipid head group interactions. Implication for understanding protein-lipid interactions. *Protein Sci.* **13,** 1503–1511
31. Olson, R., Nariya, H., Yokota, K., Kamio, Y., and Gouaux, E. (1999) Crystal structure of staphylococcal LukF delineates conformational changes accompanying formation of a transmembrane channel. *Nat. Struct. Biol.* **6,** 134–140
32. Pautsch, A., and Schulz, G. E. (1998) Structure of the outer membrane protein A transmembrane domain. *Nat. Struct. Biol.* **5,** 1013–1017
33. Monma, N., Nguyen, V. T., Kaneko, J., Higuchi, H., and Kamio, Y. (2004) Essential residues, W177 and R198, of LukF for phosphatidylcholine binding and pore formation by staphylococcal γ-hemolysin on human erythrocyte membranes. *J Biochem.* **136,** 427–431
34. Walker, B., and Bayley, H. (1995) Key residues for membrane binding, oligomerization, and pore-forming activity of staphylococcal α-hemolysin identified by cysteine scanning mutagenesis and targeted chemical modification. *J. Biol. Chem.* **270,** 23065–23071
35. Steinthorsdottir, V., Fridriksdottir, V., Gunnarsson, E., and Andrésson, O. S. (1998) Site-directed mutagenesis of *Clostridium perfringens* β-toxin. Expression of wild-type and mutant toxins in Bacillus subtilis. *FEMS Microbiol. Lett.* **158,** 17–23
36. Forti, S., and Menestrina, G. (1989) Staphylococcal α-toxin increases the permeability of lipid vesicles by cholesterol- and pH-dependent assembly of oligomeric channels. *Eur. J. Biochem.* **181,** 767–773
37. Tomita, T., Watanabe, M., and Yasuda, T. (1992) Influence of membrane fluidity on the assembly of *Staphylococcus aureus* α-toxin, a channel-forming protein, in liposome membrane. *J. Biol. Chem.* **267,** 13391–13397
38. Potrich, C., Bastiani, H., Colin, D. A., Huck, S., Prévost, G., and Dalla Serra, M. (2009) The influence of membrane lipids in *Staphylococcus aureus* γ-hemolysins pore formation. *J. Membr. Biol.* **227,** 13–24
39. Nagahama, M., Hara, H., Fernandez-Miyakawa, M., Itohayashi, Y., and Sakurai, J. (2006) Oligomerization of *Clostridium perfringens* ϵ-toxin is dependent upon membrane fluidity in liposomes. *Biochemistry* **45,** 296–302
40. McMullen, T. P. W., Lewis, R. N. A. H., and McElhaney, R. N. (2004) Cholesterol-phospholipid interactions, the liquid-ordered phase and lipid rafts in model and biological membranes. *Curr. Opin. Colloid Interface Sci.* **8,** 459–468
41. Comai, M., Dalla Serra, M., Coraiola, M., Werner, S., Colin, D. A., Monteil, H., Prévost, G., and Menestrina, G. (2002) Protein engineering modulates the transport properties and ion selectivity of the pores formed by staphylococcal γ-haemolysins in lipid membranes. *Mol. Microbiol.* **44,** 1251–1267
42. Misakian, M., and Kasianowicz, J. J. (2003) Electrostatic influence on ion transport through the αHL channel. *J. Membr. Biol.* **195,** 137–146
43. Noskov, S. Y., Im, W., and Roux, B. (2004) Ion permeation through the α-hemolysin channel. Theoretical studies based on Brownian dynamics and Poisson-Nernst-Plank electrodiffusion theory. *Biophys. J.* **87,** 2299–2309
44. Gu, L. Q., Dalla Serra, M., Vincent, J. B., Vigh, G., Cheley, S., Braha, O., and Bayley, H. (2000) Reversal of charge selectivity in transmembrane protein pores by using noncovalent molecular adapters. *Proc. Natl. Acad. Sci. U.S.A.* **97,** 3959–3964
45. Clarke, J., Wu, H. C., Jayasinghe, L., Patel, A., Reid, S., and Bayley, H. (2009) Continuous base identification for single-molecule nanopore DNA sequencing. *Nat. Nanotechnol.* **4,** 265–270